Inorg. Chem. **2004**, *43*, 4867−4879

Theoretical Analysis of the Three-Dimensional Structure of Tetrathiolato Iron Complexes

Vladislav V. Vrajmasu,† Eckard MUnck,* and Emile L. Bominaar*

Department of Chemistry, Carnegie Mellon University, 4400 Fifth Avenue, Pittsburgh, Pennsylvania 15213

Received April 2, 2004

The three-dimensional structures of a number of $[M(SR)_4]^{n-}$ complexes, where M is a 3d transition metal and R is an alkyl or aryl group, have been analyzed using density functional theory (DFT). Special attention is paid to the Fe^{II}/Fe^{III} mimics of rubredoxin. The Fe^{II} model complex $[Fe(SCH_3)_4]^{2-}$ has an equilibrium conformation with D_{2d} symmetry. The DFT energy has been decomposed into contributions for ligand–ligand and metal–ligand interactions. The latter contribution is analyzed with the angular overlap model (AOM) and constitutes the dominant stereospecific interaction in the Fe^{II} complex. The sulfur lone-pair electrons exert anisotropic π interactions on the $3d^6$ shell of Fe^{II}, which are controlled by the torsion angles, ω_i, for the rotations of the S_i–C_β bonds around the Fe–S_i axes. In contrast, the π interactions acting on the high-spin $3d^5$ shell of Fe^{III} are isotropic. As a consequence, the stereochemistry of the Fe^{III} complexes is determined by the Coulomb repulsions between the ligands and has S_4 symmetry. The electrostatic repulsions between the lone pairs of the sulfurs are an essential component of the ligand–ligand interaction. The lone-pair repulsions distort the ∠SFeS′ angles ($\delta + \delta_t$) and give rise to a correlation between δ and ω, which is confirmed by crystallographic data. Both the Fe^{II} and Fe^{III} complexes exhibit structural bistability due to the presence of low-lying equilibrium conformations with S_4 symmetry in which the complex can be trapped by the crystalline host.

1. Introduction

The metalloprotein rubredoxin, Rd, contains an $[Fe(Cys)_4]^{n-}$ site in which the iron can be in an Fe^{II} ($n = 2$, Rd_{red}) or Fe^{III} ($n = 1$, Rd_{ox}) state.[1−5] The coordination sites in Rd[6−10] and synthetic analogues[11−18] have been thoroughly investigated by crystallography, and the structure data have been reviewed recently.[19−21] The FeS_4 cores in both the native systems and analogues display similar D_{2d}-like distortions from T_d symmetry, suggesting that the deformations are an intrinsic

* Authors to whom correspondence should be addressed. E-mail: eb7g@andrew.cmu.edu (E.L.B.); emunck@cmu.edu (E.M.).

† We dedicate this paper to the memory of our graduate student Vladislav V. Vrajmasu, who died during the preparation of this paper.

(1) Palmer, G., Ed. *The Enzymes*; Academic Press: New York, 1975; Vol. 12.
(2) Lovenberg, W., Ed. *Iron−Sulfur Proteins*; Academic Press: New York, 1973; Vols. 1 and 2.
(3) Lovenberg, W., Ed. *Iron−Sulfur Proteins*; Academic Press: New York, 1977; Vol. 3.
(4) Spiro, T. G., Ed. *Iron−Sulfur Proteins*; Wiley and Sons: New York, 1982; Vol. 4.
(5) *Adv. Inorg. Chem.*; Sykes, A. G., Ed.; Academic Press: New York, 1992; Vol. 38.
(6) Watenpaugh, K. D.; Sieker, L. C.; Jensen, L. H. *J. Mol. Biol.* **1980**, *138*, 615−633.
(7) Day, M. W.; Hsu, B. T.; Joshua-Tor, L.; Park, J. B.; Zhou, Z. H.; Adams, M. W. W.; Rees, D. C. *Protein Sci.* **1992**, *1*, 1494−1507.
(8) Archer, M.; Huber, R.; Tavares, P.; Moura, I.; Moura, J. J. G.; Carrondo, M. A.; Sieker, L. C.; LeGall, J.; Romao, M. J. *J. Mol. Biol.* **1995**, *251*, 690−702.
(9) Dauter, Z.; Wilson, K. S.; Sieker, L. C.; Moulis, J. M.; Meyer, J. *Proc. Natl. Acad. Sci. U.S.A.* **1996**, *93*, 8836−8840.
(10) Min, T.; Ergenekan, C. E.; Eidsness, M. K.; Ichiye, T.; Kang, C. *Protein Sci.* **2001**, *10*, 613−621.
(11) Holah, D. G.; Coucouvanis, D. *J. Am. Chem. Soc.* **1975**, *97*, 6917−6919.
(12) Lane, R. W.; Ibers, J. A.; Frankel, R. B.; Holm, R. H. *Proc. Natl. Acad. Sci. U.S.A.* **1975**, *72*, 2868−2872.
(13) Lane, R. W.; Ibers, J. A.; Frankel, R. B.; Papaefthymiou, G. C.; Holm, R. H. *J. Am. Chem. Soc.* **1977**, *99*, 84−98.
(14) Swenson, D.; Baenziger, N. C.; Coucouvanis, D. *J. Am. Chem. Soc.* **1978**, *100*, 1932−1934.
(15) Coucouvanis, D.; Swenson, D.; Baenziger, N. C.; Murphy, C.; Holah, D. G.; Sfarnas, N.; Simopoulos, A.; Kostikas, A. *J. Am. Chem. Soc.* **1981**, *103*, 3350−3362.
(16) Koch, S. A.; Maelia, L. E.; Millar, M. *J. Am. Chem. Soc.* **1983**, *105*, 5944−5945.
(17) Maelia, L. E.; Millar, M.; Koch, S. A. *Inorg. Chem.* **1992**, *31*, 4594−4600.
(18) Silver, A.; Koch, S. A.; Millar, M. *Inorg. Chim. Acta* **1993**, *205*, 9−14.
(19) Berg, J. M.; Holm, R. H. In *Iron−Sulfur Proteins*; Spiro, T. G., Ed.; Wiley & Sons: New York, 1982; Vol. 4, pp 1−66.
(20) Meyer, J.; Moulis, J. M. In *Handbook of Metalloproteins*; Messeschmidt, A., Huber, R., Poulos, T., Wieghardt, K., Eds.; Wiley & Sons: Chichester, 2001; pp 505−517.
(21) Rao, P. V.; Holm, R. H. *Chem. Rev.* **2004**, *104*, 527−560.

10.1021/ic040049w CCC: $27.50
Published on Web 07/10/2004

property of the complexes.[15] In the previous paper of this issue,[22] we have shown that the core distortions are not a JT effect but most likely arise under the influence of the β carbons.[7,23] The electronic structure of the tetrathiolates of iron has been explored with several spectroscopic[13,15,24−48] and theoretical methods.[46,47,49−55] D_{2d} distortions split the E$\{3z^2 - r^2, x^2 - y^2\}$ ground doublet of Fe^{II} in T_d symmetry into A_1 and B_1. In a previous study, we examined the 3d orbital energies and states as a function of conformation and found that they are determined by the torsion angles, ω_i, for the rotations of the S_i-C_β bonds around the $Fe-S_i$ axes, rather than by the ∠SFeS′ angles.[46] The rotations orient the sulfur lone-pair orbitals (Figure 1) and control the spatially anisotropic π interactions between the ligands and the metal.[39,46,49,50]

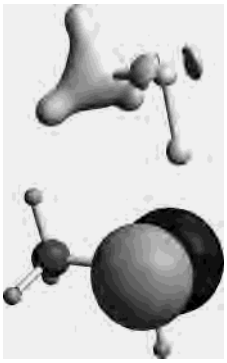

Figure 1. Upper panel shows an equidensity plot of the total electron density in H_3CSH obtained by DFT. Areas with increased charge density are visible right and left of the sulfur atom and arise from the electrons in the sulfur lone-pair orbital, shown in the lower panel.

In the present study, we determine the equilibrium conformation and electronic ground state for a number of $[M(SR)_4]^{n-}$ complexes using density functional theory (DFT)[56] and analyze how these entities evolve from the dependence of the Coulomb interactions on the structural and electronic variables. The analysis is based on a decomposition of the DFT energy into Coulomb interactions between the thiolate ligands and the $Fe(3d^6)-(SR)_i$ interaction energies (section 3.2). The metal−ligand contribution is examined in the framework of the angular overlap model (AOM) in sections 3.3 and 3.4.[57] The ligand−ligand repulsion energy is analyzed in section 3.1 and shows a complex behavior as a function of the four torsion angles, ω_i, $i = 1-4$, and the ratio, q_S/q_R, of the Mulliken charges for sulfur S and residue R.

Coucouvanis et al.[15] and Maelia et al.[17] have suggested that the deformations of the MS_4 core in $[M(SR)_4]^{n-}$ aryl complexes are caused by steric repulsions between the ortho hydrogens, *o*-H, of the aryl residues and nearby thiolate sulfurs. We propose, on the basis of an analysis of sulfur lone-pair repulsions, an alternative mechanism, which rationalizes the structures of the MS_4 units in complexes with both aryl- and alkyl-based thiolate ligands (sections 3.5 and 3.6).

(22) Vrajmasu, V. V.; Münck, E.; Bominaar, E. L. *Inorg. Chem.* **2004**, *43*, 4862−4866 (preceding article in this issue).
(23) Bertini, I.; Kurtz, D. M.; Eidsness, M. K.; Liu, G.; Luchinat, C.; Scott, R. A. *J. Biol. Inorg. Chem.* **1998**, *3*, 401−410.
(24) Buckingham, A. D.; Stephens, P. J. *Annu. Rev. Phys. Chem.* **1966**, *17*, 399−432.
(25) Phillips, W. D.; Poe, M.; Weiher, J. F.; McDonald, C. C.; Lovenberg, W. *Nature (London)* **1970**, *227*, 574.
(26) Eaton, W. A.; Lovenberg, W. *J. Am. Chem. Soc.* **1970**, *92*, 7195−7198.
(27) Eaton, W. A.; Palmer, G.; Fee, J. A.; Kimura, T.; Lovenberg, W. *Proc. Natl. Acad. Sci. U.S.A.* **1971**, *68*, 3015−3020.
(28) Peisach, J.; Blumberg, W. E.; Lode, E. T.; Coon, M. J. *J. Biol. Chem.* **1971**, *246*, 5877−5881.
(29) Rao, K. K.; Evans, M. C. W.; Cammack, R.; Hall, D. O.; Thompson, C. L.; Jackson, P. J.; Johnson, C. E. *Biochem. J.* **1972**, *129*, 1063−1070.
(30) Schulz, C.; Debrunner, P. G. *J. Phys. Colloq.* **1976**, *37*, 153.
(31) Winkler, H.; Schulz, C.; Debrunner, P. G. *Phys. Lett. A* **1979**, *69*, 360−363.
(32) Kostikas, A.; Petrouleas, V.; Simopoulos, A.; Coucouvanis, D.; Holah, D. G. *Chem. Phys. Lett.* **1976**, *38*, 582−584.
(33) Debrunner, P. G.; Münck, E.; Que, L.; Schultz, C. E. In *Iron−Sulfur Proteins*; Lovenberg, W., Ed.; Academic Press: New York, 1977; Vol. 3, pp 381−417.
(34) Moura, I.; Huynh, B. H.; Hausinger, R. P.; Le Gall, J.; Xavier, A. V.; Münck, E. *J. Biol. Chem.* **1980**, *255*, 2493−2498.
(35) Trautwein, A. X.; Bill, E.; Blaes, R.; Lauer, S.; Winkler, H.; Kostikas, A. *J. Chem. Phys.* **1985**, *82*, 3584−3593.
(36) Winkler, H.; Bill, E.; Trautwein, A. X.; Kostikas, A.; Simopoulos, A.; Terzis, A. *J. Chem. Phys.* **1988**, *89*, 732−740.
(37) Bennett, D. E.; Johnson, M. K. *Biochim. Biophys. Acta* **1987**, *911*, 71−80.
(38) Gebhard, M. S.; Deaton, J. C.; Koch, S. A.; Millar, M.; Solomon, E. I. *J. Am. Chem. Soc.* **1990**, *112*, 2217−2231.
(39) Gebhard, M. S.; Koch, S. A.; Millar, M.; Devlin, F. J.; Stephens, P. J.; Solomon, E. I. *J. Am. Chem. Soc.* **1991**, *113*, 1640−1649.
(40) Werth, M. T.; Kurtz, D. M., Jr.; Howes, B. D.; Huynh, H. B. *Inorg. Chem.* **1989**, *28*, 1357−1361.
(41) van Elp, J.; George, S. J.; Chen, J.; Peng, G.; Chen, C. T.; Tjeng, L. H.; Meigs, G.; Lin, H. J.; Zhou, Z. H.; Adams, M. W. W.; Searle, B. G.; Cramer, S. P. *Proc. Natl. Acad. Sci. U.S.A.* **1993**, *90*, 9664−9667.
(42) Rose, K.; Shadle, S. E.; Eidsness, M. K.; Kurtz, D. M.; Scott, R. A.; Hedman, B.; Hodgson, K. O.; Solomon, E. I. *J. Am. Chem. Soc.* **1998**, *120*, 10743−10747.
(43) Yoo, S. J.; Meyer, J.; Achim, C.; Peterson, J.; Hendrich, M. P.; Münck, E. *J. Biol. Inorg. Chem.* **2000**, *5*, 475−487.
(44) Volkman, B. F.; Wilkens, S. J.; Lee, A. L.; Xia, B.; Westler, W. M.; Beger, R.; Markley, J. L. *J. Am. Chem. Soc.* **1999**, *121*, 4677−4683.
(45) Knapp, M. J.; Krzystek, J.; Brunel, L. C.; Hendrickson, D. N. *Inorg. Chem.* **2000**, *39*, 281−288.
(46) Vrajmasu, V. V.; Bominaar, E. L.; Meyer, J.; Münck, E. *Inorg. Chem.* **2002**, *41*, 6358−6371.
(47) Kennepohl, P.; Solomon, E. I. *Inorg. Chem.* **2003**, *42*, 689−695.
(48) Kennepohl, P.; Solomon, E. I. *Inorg. Chem.* **2003**, *42*, 696−708.
(49) Bair, R. A.; Goddard, W. A., III. *J. Am. Chem. Soc.* **1977**, *99*, 3505−3507.
(50) Bair, R. A.; Goddard, W. A., III. *J. Am. Chem. Soc.* **1978**, *100*, 5669−5676.
(51) Norman, J. G.; Jackels, S. C. *J. Am. Chem. Soc.* **1975**, *97*, 3833−3835.
(52) Noodleman, L.; Norman, J. G.; Osborne, J. H.; Aizman, A.; Case, D. A. *J. Am. Chem. Soc.* **1985**, *107*, 3418−3426.
(53) Ueyama, N.; Sugawara, T.; Tatsumi, K.; Nakamura, A. *Inorg. Chem.* **1987**, *26*, 1978−1981.
(54) Koerner, J. B.; Ichiye, T. *J. Phys. Chem. B* **1997**, *101*, 3633−3643.
(55) Niu, S.; Wang, X.-B.; Nichols, J. A.; Wang, L.-S.; Ichiye, T. *J. Phys. Chem. A* **2003**, *107*, 2898−2907.
(56) Frisch, M. J.; Trucks, G. W.; Schlegel, H. B.; Scuseria, G. E.; Robb, M. A.; Cheeseman, J. R.; Zakrzewski, V. G.; Montgomery, J. A.; Stratmann, R. E.; Burant, J. C.; Dapprich, S.; Millam, J. M.; Daniels, A. D.; Kudin, K. N.; Strain, M. C.; Farkas, Ö.; Tomasi, J.; Barone, V.; Cossi, M.; Cammi, R.; Mennucci, B.; Pomelli, C.; Adamo, C.; Clifford, S.; Ochterski, J.; Petersson, G. A.; Ayala, P. Y.; Cui, Q.; Morokuma, K.; Salvador, P.; Dannenberg, J. J.; Malick, D. K.; Rabuck, A. D.; Raghavachari, K.; Foresman, J. B.; Cioslowski, J.; Ortiz, J. V.; Baboul, A. G.; Stefanov, B. B.; Liu, G.; Liashenko, A.; Piskorz, P.; Komáromi, I.; Gomperts, R.; Martin, R. L.; Fox, D. J.; Keith, T.; Al-Laham, M. A.; Peng, C. Y.; Nanayakkara, A.; Challacombe, M.; Gill, P. M. W.; Johnson, B.; Chen, W.; Wong, M. W.; Andres, J. L.; Gonzalez, C.; Head-Gordon, M.; Replogle, E. S.; Pople, J. A. *Gaussian 98*, revision A.11, Gaussian, Inc.: Pittsburgh, PA, 1998.
(57) Gerloch, M.; Woolley, R. G. *Prog. Inorg. Chem.* **1989**, *31*, 371−446.

2. Methods

Density functional calculations were performed using Becke's three parameter hybrid functional (B3LYP) provided by the Gaussian 98W (release A.9) software package.[56] The basis set 6-311G was used,[58] unless otherwise stated. Mulliken population analysis was employed to monitor the electron distribution. The SCF calculations were terminated upon reaching tight convergence criteria (10^{-6} rmsd in the density matrix and 10^{-8} au maximum deviation in energy). The calculations were performed on truncated models $[Fe(SCN)_4]^{2-}$ and $[Fe(SCH_3)_4]^{n-}$ ($n = 2$ or 1) of Rd_{red} and Rd_{ox} and metal-substituted species. Starting geometries for $[M(SCH_3)_4]^{n-}$ (M = Zn, Ga, $n = 2$, 1) were obtained from X-ray data for rubredoxin (reduced or oxidized). Initial geometries of tetrachlorometalates (M = Fe^{2+}, Fe^{3+}, Zn^{2+}, and Ga^{3+}) were estimated by averaging several known crystal structures for these anions. The X-ray averaged structures were first optimized using the LanL2DZ basis set and the Berny optimization procedure. The resulting geometry and electronic structure was used as a starting point for subsequent optimization using the 6-311G basis set. The results were refined by inclusion of polarization, diffuse, or both type of functions and the use of Wachters (+f) all electron basis set on the Fe center, while keeping the 6-311G basis on the nonmetals. Both nonrelaxed (modification of one geometry parameter while keeping the other ones fixed) potential energy surface (PES) scans and relaxed PES scans (modification of one geometry parameter while optimizing the others) were employed to analyze the response of the system under certain imposed distortions. The energies of the Kohn−Sham orbitals failed to reproduce the experimentally observed excitation energies and are not presented. The energies of quintet→quintet d−d transitions were calculated by (i) time-dependent DFT (TD-DFT)[59] and (ii) converging the SCF procedure in Kohn−Sham states, of which the orbital populations were altered. The two methods result in excitation energies that are equal within the accuracy of the TD-DFT method implemented in Gaussian 98 (∼0.18 eV).

3. Results and Discussion

3.1. Coulomb Repulsions between Side Chains. In this section we study the conformations that minimize the total Coulomb repulsion energy between the four $(SR)^{1-}$ side chains of the metal site in $[Fe(SR)_4]$, using an idealized $Fe(SC)_4$ model in which the FeS_4 unit has T_d symmetry, the bond angles and distances are constant, and the torsion angles, $C_iS_iFeS_{i'}$ (denoted ω_i, Figure 2B), are variable.[60] The electrostatic conformations depend on the ratio, q_C/q_S, of the charges on the carbon and sulfur atoms, which are assumed to be ω_i-independent point charges located at the C_i and S_i nuclei. The symmetry group of the potential in which the carbons move, $V(\{\omega\})$, is T_d; the argument $\{\omega\}$ denotes the set $\{\omega_1, \omega_2, \omega_3, \omega_4\}$ of torsion angles. In the limiting case $q_C/q_S \ll 1$, the repulsions between the carbon atoms can be neglected with respect to the repulsions between the carbons and the sulfurs (the DFT Mulliken charges of both sulfur and carbon are negative). Each carbon then occupies one of the three degenerate minima, located at the torsion angles

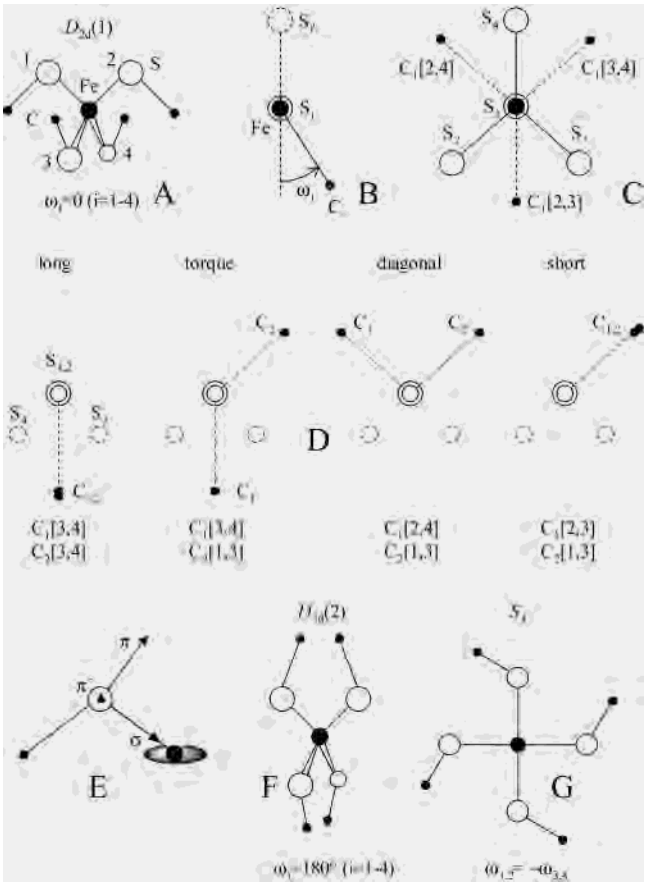

Figure 2. (A) $D_{2d}(1)$ conformation of the $[Fe(SC)_4]$ moiety at the origin of the ω axis in S_4 symmetry. The label (1) of $D_{2d}(1)$ indicates that $\omega < 90°$. (B) Definition of the torsion angle, ω_i, for the rotation of residue R_i around the S_i−Fe axis. A positive rotation is anticlockwise when viewed from S_i to Fe. (C) View along the 3-fold symmetry axis, S_1−Fe, of the tetrahedral FeS_4 core. The positions of C_1 for $\omega = 0°$, 120°, and 240°, where the repulsion between C_1 and the four sulfurs is minimum, are indicated. (D) The four possible arrangements of two carbons at the minima defined in cartoon C. (E) Spatial orientations defining the σ, π, and π' interactions in the CSFe moiety. The π' orientation, indicated by a triangular symbol, is directed perpendicular to the CSFe plane. The doubly occupied Fe $3z^2 - r^2$ orbital in the equilibrium conformation is shown. (F) $D_{2d}(2)$ conformation at the upper extreme of the torsion axis for S_4 symmetry, $\omega = 180°$. The label (2) is used to indicate that $\omega > 90°$. (G) S_4 conformation. In all cartoons: Fe = large filled circles, C = small filled circles, and S = open circles.

$\omega_i = 0°$, 120°, and 240° (Figure 2C), of the electrostatic potential generated by the charges at the S atoms. Altogether, one obtains a total of $3^4 = 81$ degenerate minima for the four carbons. The carbon−carbon repulsions, however, remove the degeneracy from the 81-fold manifold and give rise to minima with lower multiplicities. It is shown in section S.1 of the Supporting Information that the resulting minima can be classified by assigning invariance subgroups of the symmetry group T_d (Table 1). By definition, the invariance subgroup for a minimum consists of the T_d transformations that map the conformation at the minimum onto itself. In general, the order of the symmetry group, here 24 (T_d), is the product of the order of the invariance subgroup and the number of equivalent minima (section S.1). For example, the minima with D_{2d} symmetry (group order 8) are three in number and correspond to conformations such as the one shown in Figure 2A, where the S_4 axis in D_{2d} can be taken along either x, y, or z. Minima of T_d and D_2 symmetry are

(58) Frisch, E.; Frisch, M. J. *Gaussian 98 User's Reference*; Gaussian, Inc.: Pittsburgh, PA, 1999.
(59) Wiberg, K. B.; Stratmann, R. E.; Frisch, M. J. *Chem. Phys. Lett.* **1998**, *297*, 60−64.
(60) In our definition of ω, this angle is related to the conventional dihedral angle ∠S′FeSC as $\omega = 180° - ∠S'FeSC$.

Table 1. Classification of 81 Electrostatic Minima in Torsion Space $\{\omega_1, \omega_2, \omega_3, \omega_4\}$ in the Limit of Small q_C/q_S Ratio

subgroup[a]	order	#minima[b]	(1,2)[c]	(3,4)	(1,3)	(1,4)	(2,3)	(2,4)
D_{2d}	8	3	l[d]	l	d	d	d	d
S_4	4	6	t	t	d	t	t	d
C_2	2	12	l	d	t	s	s	t
C_{1h}	2	12	l	s	s	s	t	t
$C_1(1)$[e]	1	24	l	t	s	d	t	d
$C_1(2)$[e]	1	24	t	t	s	t	d	t

[a] Of T_d. [b] # indicates the number of elements (order) of a set. Values follow from $\#T_d/\#\text{Subgroup}$ ($\#T_d = 24$). Minima are generated by T_d operations on the one specified in the last 6 columns. The numbers add up to $3^4 = 81$, as explained in the text. [c] Pairs of S−C groups, (i,j) ≡ $((SC)_i,(SC)_j)$. [d] Relationship of side chains at one of the minima: l = long, t = torqued, d = diagonal, s = short, defined in Figure 2D. [e] Inequivalent sets.

lacking (Table 1) for the following reasons. T_d contains four 3-fold axes, defining operations that move one of the carbons to an unoccupied position (e.g., the carbon in Figure 2C at $\omega_i = 0°$ to 120° or 240°) and is therefore excluded as invariance group. D_2 conformations arise when the four torsion angles are equal: $\{\omega\} = \{\omega, \omega, \omega, \omega\}$. The repulsion along the D_2 coordinate has a minimum for $\omega = 0°$ (Figure 2A) and a maximum for $\omega = 180°$ (Figure 2F).[60] As a consequence, the D_2 minima have the higher, D_{2d}, symmetry that has been listed in Table 1. For $q_C/q_S \ll 1$, the total number of minima, obtained by adding the numbers listed in the third column of Table 1, is 81. The minima with the lowest repulsion energies are found to be the ones with S_4 symmetry that are characterized by two positive and two negative torsion angles, e.g., $\{\omega, \omega, -\omega, -\omega\}$ (Figure 2G).

The number of minima decreases upon increasing the carbon charges, and eventually only the six S_4 (group order 4) minima are left. In the limit $q_C/q_S \gg 1$, where the carbon−carbon interactions dominate, the carbons approach the vertexes of a tetrahedron (Figure S.1). The repulsion energy between four equal point charges, of which the motions are confined to the surface of a sphere, is a minimum in conformations where these charges describe a tetrahedron on the sphere. The S_4 conformations belong to this "spherical" set and include a tetrahedral arrangement of carbons.[61] Obviously, the tetrahedral carbon conformation minimizes the total C···C′ repulsion energy in the conformational set $\{\omega\}$, being the energy minimum of the more extended set of spherical conformations. The S_4 torsion angle in the tetrahedral carbon arrangement can be expressed as a function of $\rho = \cot(\angle S_iFeC_i)$, i.e., the cotangent of the angle between the Fe−S and Fe−C vectors in the ligands:

$$\omega = \arccos[(\rho \mp \sqrt{\rho^2 + 1})/\sqrt{2}] \qquad (1)$$

The − sign applies when $\angle S_iFeC_i \leq 180° - 2\arccos(\sqrt{(1/3)}) \approx 70.53°$, and the + sign applies in the case of a reversed inequality sign. In Rd_{red}, where $\angle S_iFeC_i \approx 32.6°$, the S_4 torsion is $\omega \approx 102°$ (Figure S.1).

(61) The existence of an S_4 conformation with the carbons occupying the vertexes of a regular tetrahedron can be demonstrated as follows. The carbon−carbon distances along the S_4 coordinate appear as $C_1C_2 = C_3C_4 \equiv d_1$ and $C_1C_3 = C_1C_4 = C_2C_3 = C_2C_4 \equiv d_2$ (Figure 2G). Since $d_1 > d_2$ for $\omega = 0°$ (Figure 2A) and $d_1 < d_2$ for $\omega = 180°$ (Figure 2F), there must exist a point on the S_4 ω axis where all six C···C′ distances are equal, i.e., $d_1 = d_2$.

Figure 3B shows the Coulomb repulsion energy between the side chains of the hypothetical Fe^{II} complex $[Fe(SCN)_4]^{2-}$ calculated as a function of the torsion angle, ω, in S_4 symmetry (dashed−dotted curve), using the atom-centered DFT Mulliken charges obtained in the ground state at $\omega = 0°$: $q_S(0)$, $q_C(0)$, $q_N(0)$.[62] The potential surface has a global S_4 minimum ($\omega \approx 100°$) and a shallow, local D_{2d} minimum ($\omega = 0°$) and exhibits a steep increase for larger values of the torsion angle due to the close contacts in two of the CN···CN′ pairs.[54] The absolute maximum is attained in the second D_{2d} structure, depicted in Figure 2F. The D_{2d} minimum is converted to a local maximum when the repulsion energies are calculated on the basis of the ω-dependent DFT Mulliken charges, $q_S(\omega)$, $q_C(\omega)$, $q_N(\omega)$, so that only the S_4 minimum is left. This property is illustrated by the solid curve in Figure 3B, which depicts the total ligand−ligand repulsion energy in the ^{5}A DFT state of parentage

$$\Psi_0 \approx |(z^2)^2(x^2 - y^2)(xy)(yz)(xz)L\rangle \qquad (2a)$$

and by the dashed curve, which represents the mean repulsion energy for the two ^{5}B states with parentages

$$\Psi_1 \approx \cos\theta\, |(z^2)(x^2 - y^2)^2(xy)(yz)(xz)L\rangle + \sin\theta\, |(z^2)(x^2 - y^2)(xy)^2(yz)(xz)L\rangle \qquad (2b)$$

$$\Psi_2 \approx -\sin\theta\, |(z^2)(x^2 - y^2)^2(xy)(yz)(xz)L(\rangle + \cos\theta\, |(z^2)(x^2 - y^2)(xy)^2(yz)(xz)L\rangle \qquad (2c)$$

The 3d orbitals in eq 2 are expressed in the Cartesian coordinates (x, y, z) defined in Figure 1 of the previous paper.[22] In this convention, the irreducible 3d sets in T_d are given by $e\{z^2, x^2 - y^2\}$ and $t_2\{xy, yz, xz\}$. L in eq 2 represents the state of the ligand electrons. The ω-dependence of the atomic charges has caused a displacement of the minimum toward a smaller angle ($\omega \approx 75°$, Figure 3B) but has not altered the S_4 symmetry of the global minimum found with fixed charges. The differences between the curves for $q_X(0)$ and $q_X(\omega)$ (X = S, C, N) in Figure 3B arise from a redistribution of the charges of the "soft" sulfur ligand as a function of ω. As a result, the C···S repulsions are diminished, and the potential is dominated by the C···C′ repulsions.[63]

In summary, the Coulomb repulsions between the thiolate ligands give rise to energy minima in conformations with S_4 symmetry on which we will focus throughout the remainder of the paper.

3.2. Decomposition of DFT Energy. In sections 3.2−4 we analyze the structure dependence of the DFT energies for the ground state and the first two excited states of $[Fe(SR)_4]^{2-}$ in terms of the Coulomb repulsions between the side chains and the interactions between the 3d electrons and the ligands. The solid curve in Figure 3A depicts the DFT

(62) The cyanide ligand was chosen to reduce the number of atoms and because the nitrogens in the linear $(SCN)^{1-}$ units do not lower the symmetry.

(63) For further details, refer to the discussion of Figure S.4B, given in section S.6.

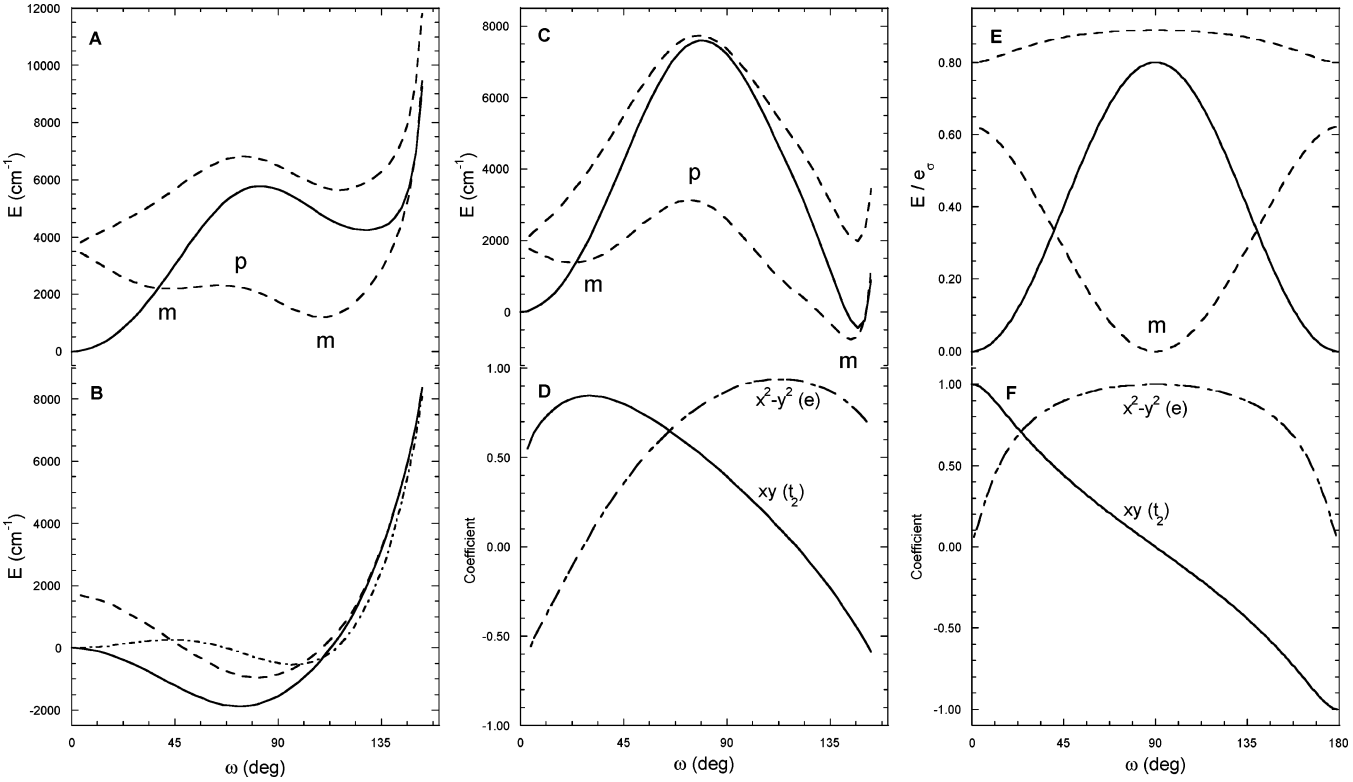

Figure 3. Energies and states of $[Fe^{II}(SR)_4]^{2-}$ as a function of torsion angle ω in S_4 symmetry. (A) B3LYP/6-311G energies of the lowest three orbital states of $[Fe(SCN)_4]^{2-}$, evaluated with bond distances and angles obtained for $\omega = 0°$. ^{5}A (solid curve) has $|d^5(z^2)|$ parentage and the ^{5}B states (dashed curves) have mixed $|d^5(x^2 - y^2)| - |d^5(xy)|$ parentages. The energy of the local, ^{5}B minimum at $\omega \approx 110°$ lies $\sim 10^3$ cm^{-1} above the global, ^{5}A minimum at $\omega = 0°$. The former corresponds to an S_4 conformation (Figure 2G) and the latter to the $D_{2d}(1)$ conformation (Figure 2A). (B) Ligand−ligand Coulomb repulsion energies, based on atom-centered Mulliken charges, q_S, q_C and q_N, in $[Fe(SCN)_4]^{2-}$. The solid curve is obtained using ω-dependent charges, $q_X(\omega)$, X = S, C, N, from DFT calculations for the state with $|d^5(z^2)|$ parentage. The dash−dotted curve is obtained using ω-independent charges, $q_S = -0.32$, $q_C = -0.19$, and $q_N = -0.28$, in unit charges, for the DFT ground state at $\omega = 0°$. The dashed curve gives the average repulsion energy for the two states with a mixed $|d^5(x^2 - y^2)| - |d^5(xy)|$ parentage, using $q_X(\omega)$ charges obtained with DFT for these states. (C) Corrected DFT energies for the lowest three orbital states of S_4 symmetric $[Fe(SCN)_4]^{2-}$ (solid, ^{5}A; dashed, ^{5}B) obtained by subtraction of the ligand−ligand repulsion energies given in B from total energies given in A. The solid and dashed curves of B were used for ^{5}A and ^{5}B, respectively. (D) Linear combination coefficients from B3LYP/6-311G calculations for the lowest ^{5}B state, $\Psi_1 \approx c_1\,\theta|^5B(xy)\rangle + c_2\,\theta|^5B(x^2 - y^2)\rangle$ (eq 2b). (E) AOM energies for ^{5}A (solid curve) and the ^{5}B states (dashed curves). Parameters used: $e_\sigma = 5000$ cm^{-1}, $e_{\pi'} = 3500$ cm^{-1}, and $e_\pi = 2000$ cm^{-1}. (F) Linear combination coefficients from AOM for the lowest ^{5}B state, $\Psi_1 = \cos\theta|^5B(xy)\rangle + \sin\theta|^5B(x^2 - y^2)\rangle$. The labels m (minimum) and p (peak) relate the features of the energy curve for the lowest ^{5}B state with those of Figure 4A

total energy of the z^2 state (eq 2a) as a function of the S_4 coordinate, ω. The function has a global minimum at $\omega = 0°$ ($D_{2d}(1)$, Figure 2A), a local maximum at $\omega \approx 80°$, a local minimum at $\omega \approx 120°$, and steeply increases to the absolute maximum at $\omega = 180°$ ($D_{2d}(2)$, Figure 2F).[64] The symmetry of the global minima for the total energy (D_{2d}) differs from the symmetry of the minimum for the ligand−ligand Coulomb energy (S_4). The minimum in the ligand−ligand repulsion energy surface (Figure 3B) nearly coincides with the local maximum in the total energy. To gain insight into the origins of the shape of the total energy function, the ligand−ligand repulsion energy was subtracted from the total energy. The difference (solid curve in Figure 3C) yields a bell-shaped curve as a function of ω, with a maximum at $\omega \approx 90°$ that is located between two minima, one at $\omega = 0°$ and a second one in the vicinity of $\omega = 180°$. In the following section it is shown that the bell shape originates from the interactions between the 3d electrons of Fe^{II} and the lone pairs of the thiolate ligands.

3.3. AOM Analysis of the Metal−Ligand Interactions in the Ground State. A systematic treatment of the influence of metal−ligand overlap on the energies and states of the 3d electrons in the open shells of transition-metal complexes is given by the Angular Overlap Model (AOM).[57] This model rests, in the 4-coordinate case, on the effective Hamiltonian

$$\mathscr{H}_{AOM} = \sum_{L=1}^{4} \mathscr{H}_{AOM}^{L} = \sum_{L=1}^{4} (e_\sigma |d_{\sigma,L}\rangle\langle d_{\sigma,L}| + e_\pi |d_{\pi,L}\rangle\langle d_{\pi,L}| + e_{\pi'} |d_{\pi',L}\rangle\langle d_{\pi',L}|) \quad (3)$$

in which the σ, π, and π' interactions, defined with respect to the individual metal−ligand frames, are described by the AO parameters, e_σ, e_π, and $e_{\pi'}$. The $d_{\xi,L}$ orbitals in the projection operators of eq 3 are quantized along the Fe−L bonds. In the case of rubredoxin, where the four ligands are identical, the AOM parameters are independent of the ligand label, L. Since the AO parameters have values ≥ 0, the expectation values of $\mathscr{H}_{AOM}$ are nonnegative, $\langle \mathscr{H}_{AOM} \rangle \geq 0$.

(64) The $D_{2d}(1)$ conformation is the global minimum of the unconstrained geometry optimizations in the full conformational spaces of both $[Fe(SCN)_4]^{2-}$ and $[Fe(SCH_3)_4]^{2-}$. Bond lengths and angles for the geometry optimized structures of $[M(SCH_3)_4]^{n-}$ obtained with various basis sets for M = Fe^{2+}, Zn^{2+}, Fe^{3+}, and Ga^{3+} in D_{2d} symmetry have been listed in Tables S.1−4 and reveal an increase in the Fe−S distance by ~0.1 Å upon 1 e reduction.

In S_4 symmetry, in which z^2 (a) does not mix with other d orbitals (b or e), the energy of the z^2 orbital is given by the diagonal element

$$\epsilon_0 = \epsilon_{z^2} = \langle 3z^2 - r^2 | \mathscr{H}_{\mathrm{AOM}} | 3z^2 - r^2 \rangle = (4/3)[(e_{\pi'} + e_{\pi}) - (e_{\pi'} - e_{\pi}) \cos 2\omega] \quad (4)$$

The z^2 energy has been plotted as a function of torsion angle, ω, in Figure 3E, together with the energies of the states of xy, $x^2 - y^2$ parentage (cf., section 3.4). We identify the energy in eq 4 with the stereospecific contribution to the metal−ligand interaction energy of the multielectronic ^{5}A state (cf., sections S.2−4). Indeed, the AOM plot for z^2 is in qualitative agreement with the graph for the repulsion-corrected DFT energy of this state (Figure 3C). The energy in eq 4 has minima at $\omega = 0°$ and 180° (both D_{2d} symmetry) and a maximum at $\omega = 90°$ (S_4). The bell shape occurs only for $\epsilon_{\pi'} > \epsilon_{\pi}$, that is, when the π' interaction normal to the FeSC plane in Figure 2E is stronger than the in-plane π interaction. The inequality is fulfilled in the case of the tetrathiolates due to the presence of the lone pairs, π', at the sulfurs (Figure 1). In the ideal case that the lone pairs of Figure 1 are the only source of π interaction ($e_{\pi'} \neq 0$ and $e_{\pi} = 0$), the AOM energies at $\omega = 0°$ and 180° vanish because the overlap between π' and z^2 is zero at these points, while the AOM energy is a maximum where the overlap is a maximum, i.e., at $\omega = 90°$.

Although the agreement between parts C and E of Figure 3 is satisfactory, establishing a quantitative relationship between DFT and AOM is a nontrivial matter and can only be approximate in nature. Sections S.2−4 of the Supporting Information take a deeper look into this problem. In section S.2 it is shown that, while the energies of both the bonding and antibonding partners of an interacting z^2−ligand orbital pair are stereospecific, the structure dependence of the energy is dominated by the antibonding orbital (z^2). Since the AOM energy of the spherically symmetric high-spin Fe^{III} (d^5) ion is independent of ω (section S.4), the stereospecificity of the interactions between the multielectronic ion Fe^{II} (d^6) and the ligands is dictated by the interactions of the minority-spin-carrying d electron.

A comparison of parts E and A of Figure 3 shows that the bistability π'−z^2 interaction is removed by the ligand−ligand repulsions, which transform the global minimum at $\omega = 180°$ into a local minimum with S_4 symmetry in Figure 3A.

3.4. AOM Analysis of the Metal−Ligand Interactions in the Excited States. The DFT energies of the lowest three states of the model $[Fe(SCN)_4]^{2-}$ have been plotted in Figure 3A versus the torsion angle, ω, in S_4 symmetry. These states include ^{5}A(z^2) (eq 2a), discussed in section 3.3, and the two ^{5}B states of xy, $x^2 - y^2$ parentage (eqs 2b, c). The latter appear as nearly degenerate levels at $\omega = 0°$ (D_{2d}) but are split under the influence of the S_4 distortion for $\omega > 0°$. The energy (ϵ_1) of the lower branch crosses the z^2 level at $\omega \approx 37°$ whereupon the ground state becomes a linear combination of xy and $x^2 - y^2$. In accordance with the theoretical prediction, a ground state of this composition has been deduced from MCD studies[39] of the S_4 complex $[Fe(SC_6H_4\text{-}2\text{-}Ph)_4]^{2-}$, with $\omega \approx 132°$.[18,60] Figure 3C depicts the side-chain-repulsion-corrected DFT energies of the lowest three states of $[Fe(SCN)_4]^{2-}$.

To gain insight into the dependencies of the energies and compositions of the ^{5}B states on torsion angle, ω, we have performed an AOM analysis of the interaction between xy and $x^2 - y^2$.[65] The energy eigenvalues of the two-dimensional secular problem can be written as an analytical function of ω in S_4 symmetry

$$\epsilon_{1,2}(\omega) = \langle \Psi_{1,2} | \mathscr{H}_{\mathrm{AOM}} | \Psi_{1,2} \rangle = (1/9)[6e_{\sigma} + 8(e_{\pi'} + e_{\pi}) + 4(e_{\pi'} - e_{\pi}) \cos 2\omega \mp 2\{9e_{\sigma}^2 - 12e_{\sigma}(e_{\pi'} + e_{\pi}) + 4(e_{\pi'} + e_{\pi})^2 + 14(e_{\pi'} - e_{\pi})^2 + 8(e_{\pi'} - e_{\pi})(2(e_{\pi'} + e_{\pi}) - 3e_{\sigma}) \cos 2\omega + 2(e_{\pi'} - e_{\pi})^2 \cos 4\omega\}^{1/2}] \quad (5)$$

where the $\mp$ signs have been chosen such that $\epsilon_2 \geq \epsilon_1$. A typical set of AOM energy curves for ^{5}B states has been plotted in Figure 3E. The minimum and maximum of the dashed curves at $\omega = 90°$ have a ^{5}B($x^2 - y^2$) state and a ^{5}B(xy) state and correspond with a zero in $\langle x^2 - y^2 | p_{\pi'} \rangle$ and a maximum in $\langle xy | p_{\pi'} \rangle$, respectively. The AOM parameters used in Figure 3E, $e_{\sigma} = 5000\ \mathrm{cm}^{-1}$, $e_{\pi'} = 3500\ \mathrm{cm}^{-1}$, and $e_{\pi} = 2000\ \mathrm{cm}^{-1}$, were estimated from the side-chain-repulsion-corrected DFT energies for the states in Figure 3C, as described in section S.5, based on the relationship between the side-chain-corrected total DFT energy and the AOM energy, established in section S.4.

A comparison of parts E (AOM) and C (DFT) of Figure 3 reveals a number of similar features: (1) The orbital ground state changes from z^2 at $\omega = 0°$ and 180° to a linear combination of $x^2 - y^2$ and xy in the central part of the ω scale. (2) The energy splitting $\epsilon_2 - \epsilon_1$ has minima at $\omega \approx 0°$ and 180° and a maximum at 90°. (3) The energy curves for the three states are (approximately) symmetric around $\omega = 90°$. (4) ϵ_2 has a maximum at ~90°. The major difference between the two figures is the value of ϵ_1 at $\omega \approx 90°$, which is a minimum of the $\epsilon_1(\omega)$ function obtained by the AOM (labeled m, minimum) and a local maximum according to DFT (labeled p, peak).

In passing from Figure 3E through 3C to 3A, we notice the following modifications. The molecule is tristable in the AOM due the degeneracy of the energy minima for ^{5}A (2×) and ^{5}B (Figure 3E). In the next section we show that the ligand−ligand interactions that arise from the spatial anisotropies (lone pairs) of the charge distributions at the sulfur centers (Figure 1) are given by the function in Figure 4A. Addition of the lone-pair repulsions (Figure 4A) to the AOM energy (Figure 3E) converts the ^{5}B minimum (labeled m) into two minima (m in Figures 3C and 4A) that are interspersed by a peak (p). The ^{5}B (S_4) minimum, m, on the right of Figure 3C is raised in energy by the atom-centered-charge repulsions relative to the minimum for $^5A_1$ (D_{2d}) and

(65) The elements of the interaction matrix of $\mathscr{H}_{\mathrm{AOM}}$ in S_4 symmetry have been listed in section S.3 of the Supporting Information.

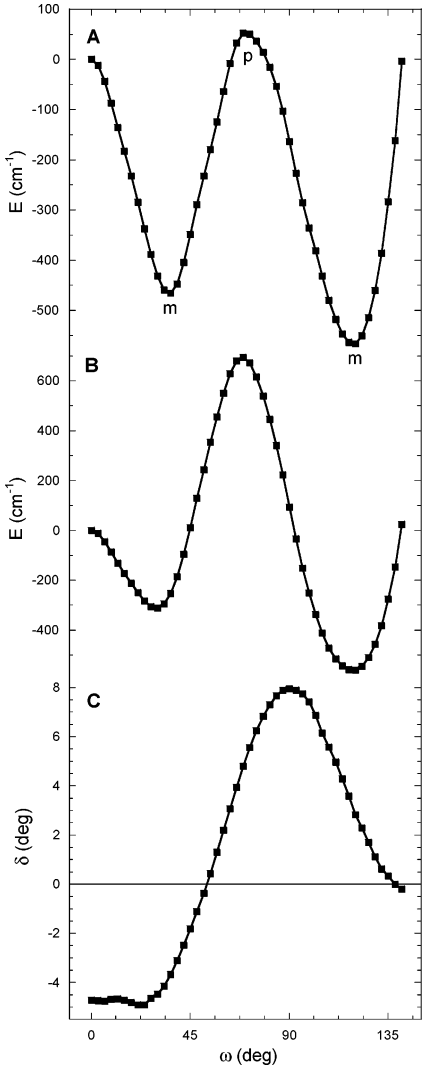

Figure 4. Energy and bond angle δ of $[Fe^{III}(SCH_3)_4]^{1-}$ as a function of torsion angle ω in S_4 symmetry. (A) B3LYP/6-311G energies obtained from a relaxed scan. (B) B3LYP/6-311G energies obtained from a scan in which only δ was optimized. (C) Optimized bond angles, $\delta_{min}(\omega)$, in the relaxed structures obtained from scan A. Angle δ is defined as $\angle SFeS' - \delta_t$ where $\delta_t \approx 109.47°$. Labels p (peak) and m (minimum) establish a relationship with the extremes in the low-energy branch of ^5B in Figure 3A, C.

converted into a low-lying excited-state minimum (Figure 3A). Although the equilibrium conformation with D_{2d} symmetry ($\omega = 0°$) has the lowest energy, the molecule can be locked in either of the extremes under the influence of an appropriate host because the energy gap between the minima for ^5B (S_4) and $^5A_1$ (D_{2d}) is small. Indeed, the majority of $[Fe^{II}(SR)_4]^{2-}$ complexes has either a (pseudo) D_{2d} or S_4 symmetry (cf., section 3.6).

Figure 3D presents the linear combination coefficients for excited state 1 (eq 2b) as a function of ω in S_4 symmetry obtained by DFT calculations for the model complex $[Fe(SCN)_4]^{2-}$. Figure 3F shows the composition of ^5B state 1 obtained by the AOM, using the parameters of Figure 3E. ^5B state 2 is the vector normal to state 1 in the space spanned by $x^2 - y^2$ and xy and has not been indicated. The ω-dependences of the state compositions derived from the DFT and AOM calculations show similar trends. The coefficients for $x^2 - y^2$ and xy have, respectively, a maximum and a zero near $\omega \approx 90°$. The maximum and zero coincide exactly in the case of the AOM, because of normalization, and only approximately so in the case of DFT, due to the admixture of ligand orbitals. The coefficients of $x^2 - y^2$ and xy, respectively, decrease and increase toward the limits of the ω scales displayed in Figure 3D, F. The orbital components $x^2 - y^2$ and xy of state 1 have equal weights at the crossing of the curves, and the AOM coefficient of $x^2 - y^2$ eventually vanishes at $\omega = 0°$ and 180°. The composition of the DFT state shows a more complex behavior in the left margin because, under the prevailing condition of near degeneracy, these states are susceptible to minor perturbations. Although being qualitatively similar, a quantitative comparison of the DFT and AOM results divulge considerable differences in the locations of the zeroes, extremes, and crossovers. These differences are especially evident at $\omega = 90°$ where $\mathscr{H}_{AOM}$ has D_{2d} symmetry.[66] Since D_{2d} symmetry excludes mixing of $x^2 - y^2$ (b_1) and xy (b_2), these orbitals cannot mix in the AOM at $\omega = 0°$, 90°, and 180° (Figure 3F). On the contrary, the DFT states are considerably mixed at the 90° angle (Figure 3D), indicating that the lower symmetry of the system (S_4), which is truncated in the AOM treatment, comes to expression at the DFT level of description. Application of Figure 3F to the S_4 complex $[NEt]_2 \cdot [Fe(SC_6H_4\text{-}2\text{-}Ph)_4]$ ($\omega = 132°$)[18] yields the mixing coefficients 0.9 ($x^2 - y^2$), 0.2 (xy), and 0.4 (ligand) and shows that the orbital ground state of this complex does not have a pure E (T_d) parentage.

The present study supports the conclusion of the qualitative AO analysis reported by Gebhard et al.[39] that the torsion angles, ω_i, are the principal determinants of the ligand-field states in tetrathiolato iron complexes and confirms that the ground state of Fe^{II} in S_4 symmetry alternates between ^5A and ^5B at $\omega \approx 45°$ and 135°. Interestingly, the S_4 complex $[NEt]_2 \cdot [Fe(SC_6H_4\text{-}2\text{-}Ph)_4]$, for which a remarkably complete set of electronic structure data is available,[39] has a torsion angle located in the vicinity of a level crossing ($\omega \approx 132°$)[16,60] but exhibits nonetheless a sizable $^5A(z^2) - {}^5B(x^2 - y^2, xy)$ splitting ($\epsilon_{z^2} - \epsilon_1 \approx 1400\ cm^{-1}$).[39] Gebhard et al. have argued that since the $^5A - {}^5B$ splitting is not likely the result of S−Feπ interactions, the gap must be due to S−Feσ interactions. The S−Feσ orbital is canted relative to the Fe−S vector, with an angle that depends on geometrical factors such as the angle $\theta = \angle FeSC - 90°$. Indeed, the angular arrangement prevailing in the phenyl complex was found to stabilize the $x^2 - y^2$ orbital with respect to z^2, in agreement with the $x^2 - y^2$ character of the ground state that was inferred from the single-crystal magnetooptical data for this system. A quantitative verification of this mechanism would be desirable. Unfortunately, an evaluation of the S−Feσ interactions in the framework of the AOM is rather involved for the following reasons. First, a canted S−Feσ orbital may contribute to both the e_σ and $e_{\pi,\pi'}$ parameters. Hence, a full overlap analysis would require a refinement of the AOM by

(66) A rotation of the AOM axes in Figure 2E by 90° interchanges π and π' but leaves the D_{2d} symmetry of the Hamiltonian unchanged.

specifying the dependencies of the e parameters on the relevant bond angles. Second, the orbital ground state is an admixture of $x^2 - y^2$ and xy, which would further complicate a comprehensive AO analysis. Therefore, we present here only the AOM (Figure 3E) and DFT (Figure 3A) predictions for the $^5A - {}^5B$ splitting in the $[Fe^{II}(SCN)_4]^{2-}$ model at the torsion angle, $\omega \approx 132°$, in the phenyl complex, i.e., 900 and 1700 cm^{-1}, respectively. The predicted ground-state term, $^5B(x^2 - y^2, xy)$, is in accordance with experiment,[39] and the excitation energy computed for $^5A(z^2)$ is off by only <35%. The good agreement corroborates the notion that the 3d orbitals in $[Fe^{II}(SR)_4]^{2-}$ are not sensitive to the nature of ligand residue, R.

3.5. Intrinsic Stereochemistry of Iron(III) with a Tetracysteinate Ligation. The spherical orbital symmetry of the parent atomic ground state, ^6S, of Fe^{III} gives rise to stereounspecific interactions between the iron and the lone pairs of the sulfurs.[67] As a consequence, the Fe^{III} coordination site distorts easier than the Fe^{II} site under the influence of weak forces, such as those acting between the ligands. To investigate these interactions ($<10^3$ cm^{-1}), we have scanned the DFT energy of the model $[Fe^{III}(SCH_3)_4]^{1-}$ along the torsion coordinate ω in S_4 symmetry by performing geometry optimizations for given values of ω with respect to the remaining coordinates (Figure 4A). Unlike the case of Fe^{II}, where there is a global energy minimum at $\omega = 0°$ (D_{2d} symmetry) and a local minimum at $\omega \approx 135°$ (S_4), there are now two minima with S_4 symmetry, a local one at 35° and a global one at 115°, which are interspersed by maxima at 0°, 90°, and 180°.[68,69] In section S.6 we demonstrate that the pattern of minima and maxima in Figure 4A cannot arise from repulsions between the atom-centered charges on the ligands.

Although all structure parameters show some variations in the relaxed scan of Figure 4A, only the ∠SFeS′ bond angles exhibit a marked dependence on ω. The results for the ∠SFeS′ angles that are bisected by the S_4 axis, $\delta_{min}(\omega)$, are shown in Figure 4C. The figure shows that δ_{min} is negative at $\omega = 0°$, changes sign at $\omega \approx 50°$, and returns again to zero at $\omega \approx 140°$. The distortions correspond, respectively, to elongation, perfect tetrahedral symmetry, and compression of the FeS_4 core along the S_4 axis. To verify that the δ distortion has an essential effect on the energy, we have also performed a nonrelaxed scan along the ω axis, in which only δ was optimized. The results for the energy and δ_{min} are shown in Figures 4B and S.5, respectively, and are indeed similar to those of the full scan (Figure 4A, C).

In a first attempt to explain the relationship between δ and ω, we investigated the possibility that the nontetrahedral values of δ arise from electrostatic repulsions between the carbons. The sums of C···C′ repulsion energies in the $D_{2d}(1)$ (Figure 2A) and $D_{2d}(2)$ (Figure 2F) conformations decrease by, respectively, decreasing and increasing δ, because the carbons then approach the vertexes of a tetrahedron where the C···C′ repulsion energy is minimum. Thus, the C···C′ repulsions yield an elongation of the FeS_4 unit for $D_{2d}(1)$ and a compression for $D_{2d}(2)$. In S_4 symmetry, the ω-ranges with C-induced elongation and compression meet at $\omega \approx 102°$, i.e., the torsion angle where the carbons form a perfect tetrahedron (section 3.1). The latter arrangement minimizes the total C···C′ repulsion energy, so that the forces that distort the tetrahedral FeS_4 unit are eliminated. Thus, $\delta = 0°$ for, and only for, $\omega \approx 102°$. In contrast, the DFT curve for $\delta(\omega)$ in Figure 4C has two zeroes and a maximum at $\omega \approx 100°$, close to where a zero for C···C′ repulsion is predicted. Hence, the C···C′ repulsion mechanism for explaining the ω dependence of the DFT energy of $[Fe(SCH_3)_4]^{1-}$ has to be abandoned.

An additional piece of evidence, relevant for extracting the physical origin of the double-well potential in Figure 4A, is provided by ω scans of the metal-substituted species $[M(SCH_3)_4]$, where M is the spherical ion Ga^{3+} or Zn^{2+} (Figure S.6A, B). Bond lengths and angles obtained with various basis sets for the geometry optimized $D_{2d}(1)$ conformations of $[M(SCH_3)_4]^{n-}$ with $M = Fe^{2+}$, Zn^{2+}, Fe^{3+}, and Ga^{3+} have been listed in Tables S.1−4 and reveal consistently the presence of elongated MS_4 cores. The curves for $\delta_{min}(\omega)$ and energy (not shown) for these metals are remarkably similar and suggest that the mechanism underlying the stereochemistry of the MS_4 core is ligand based. This suggestion raises the question as to which ligand fragments are responsible for the stereospecific interactions. This issue was analyzed by scanning models in which the methyl groups in $[Fe^{3+}(SCH_3)_4]^{1-}$ are replaced by cyanide or fluoride. The results are similar to those for methyl and suggest that the thiolate sulfurs are the source of the stereochemistry of the trivalent iron complexes.

Given the considerable strength of Coulomb forces between proximal charges, it is desirable to analyze the repulsions between the sulfur atoms in further detail. The energy of the repulsions between the sulfurs is independent of torsions, ω, around the Fe−S axes when the S atoms are represented by single point charges on the rotation axes. This description of the charges, however, is incomplete and has to be refined by one that incorporates the stereospecific Coulomb interactions, arising from the spatial anisotropies of the electronic charges at the sulfurs, notably those of the lone pairs (Figure 1). Adopting a description in which the charges in the lone pairs are placed at the extremes of dumbbells that are centered at the sulfur atoms (Figure 5), we obtain the potential surface for the lone-pair Coulomb repulsion energy, $E_{LP}(\omega,0)$, shown in Figure 6A, where the ∠SFeS′ bond angles are taken as in a perfect tetrahedron.[70] The extremes in Figure 6A have been labeled with numerals to identify them with the lone-pair conformations of Figure 5 and exhibit a similar pattern as those

(67) The sum of the AOM energies for the five 3d orbitals is independent of ω; cf., eq S.4.1, section S.4.

(68) The maximum at 180° lies outside the plot range shown.

(69) DFT frequency analysis of the oxidized state shows that the $D_{2d}(1)$ conformation is a saddle point with a negative frequency for the A_2 torsion mode. This result confirms that $\omega = 0°$ is a maximum of the energy function in Figure 4A.

(70) These calculations were performed with a MATHEMATICA code written for this purpose.

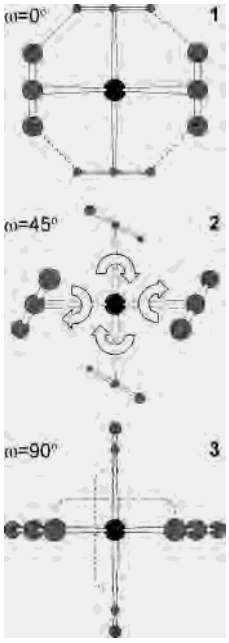

Figure 5. Sulfur lone-pair arrangements in an $[M(SR)_4]$ complex having an S_4 axis (R is not indicated) and a T_d-symmetric MS_4 core. The dashed lines indicate close contacts between the lobes of the sulfur lone pairs that are indicated by dumbbells. The numerals correspond to those indicated in Figures 6, 7, S.5, and S.7.

in Figure 4A. The two points labeled 1 (as well as those labeled 2) are equivalent in the lone-pair model but not entirely so in the DFT model of the molecule due to second neighbor repulsions (see below). Subsequently, we optimized $E_{LP}(\omega,\delta)$ with respect to δ for given values of ω, in analogy with the procedure followed in Figures 4B and S.5, and obtained Figure 6B for the optimized bond angles, $\delta_{min}(\omega)$, and Figure 6C for the corresponding energies, $E(\omega,\delta_{min}(\omega))$. The δ-optimized extremes have been labeled with primed numerals in the figures. The δ_{min} values obtained with the dumbbell model and with DFT exhibit similar trends as a function of ω, as can be seen by comparison of Figures 6B and 4C. The FeS_4 unit is elongated along the S_4 axis for $\omega = 0°$ ($\delta < 0°$) due to the repulsions in the close contacts between the lone pairs at the sulfurs in the upper and lower layer of Figure 5, top (dashed lines); whereas, in the $\omega = 90°$ conformation (Figure 5, bottom), where there are close intralayer contacts, the core unit is compressed ($\delta > 0°$). The FeS_4 unit is perfectly tetrahedral ($\delta_{min} = 0°$) at intermediate torsion angles, $\omega \approx 45°$ and 135° (Figure 5, middle).

Surprisingly, a comparison of Figure 6C, A reveals that the δ-optimized lone-pair repulsion energy, $E_{LP}(\omega,\delta_{min}(\omega))$, has minima at the torsion angles where $E_{LP}(\omega,0)$ has maxima and vice versa. To analyze what causes the exchange of extremes, we have plotted the energies for the dumbbell model, $E_{LP}(\omega,\delta)$, as a function of δ in Figure 7 for the three torsion angles considered in Figure 5. The values of the energy function $E_{LP}(\omega,0)$ for $\omega = 0°$, 45°, and 90° have been indicated on the vertical, $\delta = 0°$ axis of Figure 7 and are labeled with the numerals used in Figure 6A. Each of these points lies on a parabolic

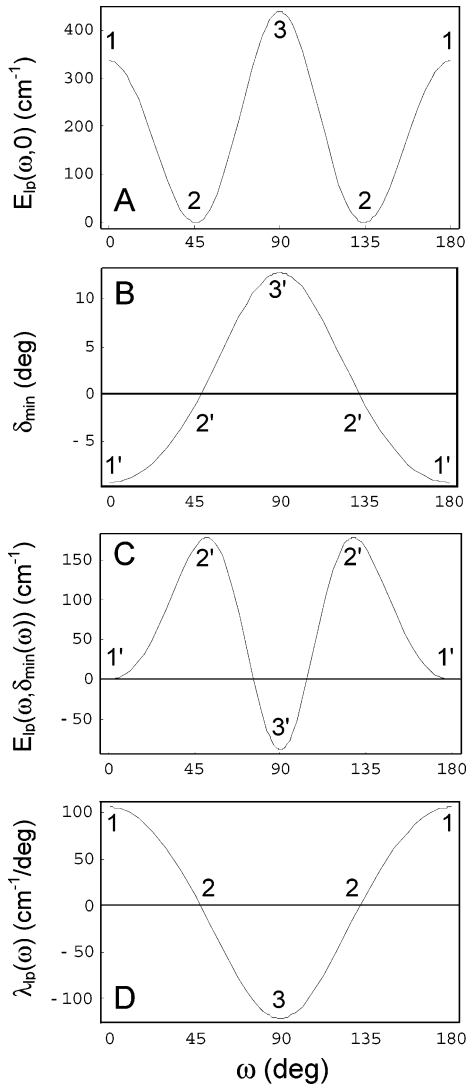

Figure 6. Results obtained with the dumbbell model for the electrostatic repulsion energy between the lone-pair electrons of the sulfurs in the MS_4 core of $[M(SR)_4]$ as a function of the torsion angle, ω, in S_4 symmetry. The numerals correspond to the dumbbell arrangements defined in Figure 5. Unprimed numerals refer to a T_d-symmetric MS_4 core ($\delta = 0°$) and primed ones to δ-optimized, D_{2d}-symmetric MS_4 cores. (A) Dumbbell repulsion energy, $E_{LP}(\omega,0)$, for a T_d-symmetric MS_4 core. (B) Optimized $\delta_{min}(\omega)$ value, obtained by minimization of the dumbbell repulsion energy at torsion ω. (C) Dumbbell repulsion energy, $E_{LP}(\omega,\delta_{min}(\omega))$, for the optimized $\delta_{min}(\omega)$ angle. (D) Vibronic coupling constant, λ_{LP}, defined in eq 6b. Parameters used: $q = -0.55$, in atomic charge units and $K = 0$ (see text).

function that is approximately of the form

$$E_{LP}(\omega,\delta) \approx \epsilon_0(\omega) + \lambda_{LP}(\omega)\delta + K_{LP}\delta^2 \qquad (6a)$$

K_{LP} is a force constant and the lambda parameter denotes the derivative,

$$\lambda_{LP}(\omega) = \left(\frac{dE_{LP}}{d\delta}\right)_0 \qquad (6b)$$

which is commonly referred to as a vibronic coupling constant.[71] λ_{LP} is a function of the torsion angle and has been plotted in Figure 6D. Accordingly, the parabolic potential

(71) Bersuker, I. B.; Borshch, S. A. *Adv. Chem. Phys.* **1992**, *81*, 703−782.

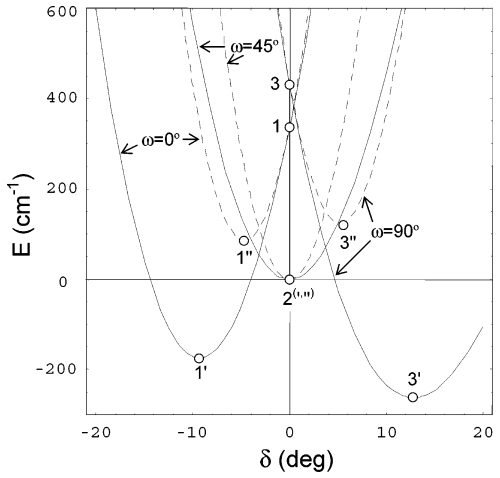

Figure 7. Dumbbell repulsion energy, $E_{LP}(\omega,\delta)$, versus the ∠SFeS′ bond angle change, δ, for selected values of ω and different values for force constant K_{eff}. The unprimed, doubly primed, and singly primed numerals label the δ-optimized minima for an infinitely large, an intermediate, and a small value for K_{eff}, respectively. The extremes have been labeled with the same numerals as in Figure 6. Notice the difference in the curvatures of the dashed and the solid curves, due to changes in K_{eff}, and the ensuing interchange of minima and maxima. Parameters used: $q = -0.55$, in atomic charge units, $K = 0$ (solid curves), and $K = 6$ cm^{-1}/deg^2 (dashed curves).

surfaces have ω-dependent minima, located at

$$\delta_{min}(\omega) = -\frac{\lambda_{LP}(\omega)}{2K_{LP}} \tag{7a}$$

The energies at the minima are given by

$$E_{LP,min}(\omega) \equiv E_{LP}(\omega,\delta_{min}(\omega)) \approx \epsilon_0(\omega) - \frac{\lambda_{LP}^2(\omega)}{4K_{LP}} \tag{7b}$$

The potential energy minima are located at $\delta_{min} < 0°$ (elongation), $\delta_{min} = 0°$ (no distortion), and $\delta_{min} > 0°$ (compression) for $\lambda_{LP} > 0$, $\lambda_{LP} = 0$, and $\lambda_{LP} < 0$, respectively. As λ_{LP} is a function of ω, the torsion angle determines the sign of ∠SFeS′ bond angle distortion: there is elongation for $\omega < 45°$ and $\omega > 135°$, compression for $45° < \omega < 135°$, and no distortion (i.e., FeS_4 has tetrahedral symmetry) for $\omega \approx 45°$ and $\omega \approx 135°$. The δ-distorted minima, 1′ and 3′ (Figure 7), have lower energies than the undistorted conformations, 1 and 3, obtained for the same values of ω (eq 7b). In general, it follows from eq 7 that large vibronic couplings and small force constants lead to large distortions and large stabilization energies. In the present case, the parameters are such that the distorted conformations 1′ and 3′ have been lowered in energy to the extent that their energies are below that of the undistorted conformation $2 = 2'$ (Figure 7), leading to the pattern of extremes in Figure 6C.

At this juncture, the force constant, K_{LP}, derives entirely from the Coulomb repulsions between the lone pairs. This description of the elastic forces, however, is incomplete. Consider, for example, the energy minimized structure of $[FeCl_4]^{1-}$, a system without lone pairs. The molecule has tetrahedral symmetry; hence, there are additional elastic forces at work that have the propensity to maintain iron in a T_d-symmetric coordination and which can be formulated as $E_{elas}(\delta) = K\delta^2$. This term, together with K_{LP}, yield a larger, effective force constant, $K_{eff} = K + K_{LP}$, that replaces K_{LP} in eq 6a if one passes to the complete description. As a consequence, the distortions and their associated energies are diminished (cf., eq 7), and the original energy order is restored. For example, the energies of the minima, 1″ and 3″, of the broken curves in Figure 7 that were calculated after adding E_{elas} with $K = 5$ cm^{-1}/deg^2 are greater than the energy of the unchanged conformation $2'' = 2$. The functions $(E_{LP} + E_{elas})(\omega,\delta'_{min}(\omega))$ and $\delta'_{min}(\omega)$ have shapes similar to those of the functions shown in Figure 6A, B, respectively, but with smaller amplitudes.[72]

To account for the differences between Figure 6A, B (dumbbell model) and Figures 4B and S.5 (DFT), we refined the E_{elas}-extended dumbbell model by describing the sulfur ligands with three charges: charge $q_S - 2q$ at the center (Figure 5) and charges q at the extremes of the dumbbells, with q_S being the Mulliken charge of the sulfurs, and by adding the Coulomb repulsion energies of the C···C′ and C···S interactions, based on atom-centered Mulliken charges, q_C and q_S. The spatial extension of the dumbbells was estimated from the S 3p orbital radius to be about 2 Å. The result for the δ-optimized ω scan for the energy $E(\omega,\delta_{min}(\omega))$ (Figure S.7A) and bond angle change, $\delta_{min}(\omega)$, (Figure S.7B) show a striking resemblance with the DFT curves in Figures 4B and S.5. Unlike the simplified dumbbell model, the refined model properly assigns different energies to the local minimum on the left and the global minimum on the right. The energy difference arises from the C···C′ repulsions, which are lower in the right minimum (∼125°), because of its vicinity to the angle $\omega \approx 102°$, where the carbons occupy the vertexes of a tetrahedron (section 3.1), than in the left minimum (∼35°). The C···C′ repulsions increase rapidly for $\omega > 125°$, that is, upon approaching the sterically encumbered $D_{2d}(2)$ conformation in Figure 2F. To mitigate the increase in the C···C′ repulsions, the δ angle has the propensity to open, leading to a shift of the zero point of the function $\delta_{min}(\omega)$ toward larger values of ω, e.g., from 130° in Figure 6B to $\omega > 140°$ in Figure S.7B. A comparison of Figure S.7A, B with Figures 4B and S.5 also reveals that the local energy minimum 2″ at ∼35° and the zero point 2″ of δ_{min} at ∼60° obtained with the refined dumbbell model coincide with the positions of these points in the DFT results. This feature is unique for the refined model and is lacking in the simplified model, which has energy minima at the angular zeroes (2 and 2′ in Figure 6A, B). Due to this displacement, the FeS_4 core is predicted to be elongated ($\delta_{min} < 0°$) at the local minimum, 2″ on the left of Figure S.7A. Similarly, the global energy minimum, 2″ on the right of Figure S.7A, is located left of the corresponding angular zero, 2″ on the right of Figure S.7B, and has, therefore, a compressed FeS_4 core ($\delta_{min} < \delta_t$).

We have investigated the energies of both the sulfur lone-pair interactions (this section) and the repulsions between the atom-centered charges of the ligands (section 3.1). To address the question as to the relative importance of the two

(72) The prime in δ'_{min} indicates the minimum of the E_{elas}-extended model.

Table 2. Optimized $\delta + \delta_t$ Angles in $[M(SR)_4]^{n-}$ ($n = 1, 2$) for $D_{2d}(1)$ Conformation from B3LYP/6-311G Calculations

	M			
system	Fe^{3+}	Ga^{3+}	Fe^{2+}	Zn^{2+}
$[M(SCH_3)_4]^{n-}$	104.8[a]	102.6	106.0	104.4
$[M(SCN)_4]^{n-}$	102.3	99.3	94.8	97.8
$[M(SF)_4]^{n-}$	103.0	101.4	94.5	93.9
$[M(SPh)_4]^{n-}$	99.1	95.3	97.0[b]	94.8

[a] Angles in degrees. [b] Experiment: 99.6°.

interactions, we have listed the atomic Mulliken charges in Table S.5. The sulfur charges, $|q_S|$, decrease in the order Me > Ph > CN ≈ F. For example, in the Fe^{III} case, q_S is −0.45 for R = CH_3 and −0.15 for R = CN. The changes in q_S are balanced by the charges of the terminal groups, R, which increase from −0.12 (CH_3) to −0.40 (CN). A large value for q_S and a small value for q_R result in a weak atom-centered charge R···R′ repulsion, illustrated in Figure S.4C by the potential for R = CH_3, and a dominant lone-pair repulsion (Figure 4A for CH_3). In contrast, a small value for q_S and a large value for q_R, as found in the case of R = CN, give rise to a dominant R···R′ contribution, $E_{R-R} \approx q_R^2$, (Figures S.4B and 3B, solid curve). We have investigated the influence of replacing R = Me by Ph, F, or CN on angle δ in the $D_{2d}(1)$ conformation of the model complex $[Fe(SR)_4]^{n-}$, $n = 1, 2$ (Table 2). Also included are the results for Zn^{2+} and Ga^{3+}, which have radial extensions similar to those of Fe^{II} and Fe^{III}, respectively (Table S.6). The terminal groups F, CN, and to a lesser extent, phenyl give rise to larger distortions of the δ angle than methyl does. The angular distortions correlate with the atomic charges listed in Table S.5. A charge shift from S to R, reducing the S···S′ repulsions, "softens" the angular coordinate δ and enhances the R···R′ repulsion. Together, these factors lead to an elongation of the MS_4 unit and rationalize that these units in $[M(SR)_4]^{n-}$ for R = F, CN, and Ph are more distorted than for Me.

3.6. Crystallographic Test of Predicted Structural Regularities. 3.6.1. Selection of Complexes. We have performed a search in the Cambridge Structural Database (CSD) for homoleptic metal complexes of the form $[M(SR)_4]^{n-}$, where M^{4-n} is either a 3d transition metal ion or Cd^{2+} and SR^{1-} is a monodentate thiolate ligand. All complexes with M = Fe were retained in the search, whereas complexes with M ≠ Fe were only admitted if they had either a (pseudo) D_{2d} or (pseudo) S_4 symmetry. The latter criterion eliminated a small number of complexes with no identifiable symmetry higher than C_1. Complexes that appeared in the CSD without 3D structure data were discarded. We also excluded complexes of bidentate ligands, RS_2, because our theoretical predictions are based on the premise that the relative motions of the four ligands are not constrained by covalent linkages. The selected complexes have been listed in Table S.7 of the Supporting Information, together with the symmetry labels of their (idealized) structures.

3.6.2. Symmetry of Equilibrium Conformation. The theoretical analysis presented in this paper predicts that the structure of a $[Fe(SR)_4]^{n-}$ complex is bistable in both the ferrous and ferric state. For Fe^{II}, there is a global, $D_{2d}(1)$ minimum and a local, $S_4(2)$ minimum (Figure 3A), while for Fe^{III}, there is a global, $S_4(2)$ minimum and a local, $S_4(1)$ minimum (Figure 4A). Here, like in Figures 2A, F, the labels "(1)" and "(2)" designate that 0° ≤ ω ≤ 90° and 90° < ω ≤ 180°, respectively. Since the structural predictions for the Fe^{III} complexes are based on an analysis of ligand−ligand interactions, we anticipate that they also apply to the $[M(SR)_4]^{n-}$ complexes of the spherically symmetric ions Mn^{2+} ($3d^5$), Zn^{2+} ($3d^{10}$), and Cd^{2+} ($4d^{10}$). The Fe^{II} complexes in Table S.7 assume the conformations "$D_{2d}(1)$" (1×), $S_4(2)$ or "$S_4(2)$" (4×), "$D_{2d}(1,2)$", defined by the approximate torsion angles (0°, 0°, 180°, 180°) (1×), and C_1 (1×).[73] The spherical ions Mn^{2+}, Fe^{3+}, Zn^{2+}, and Cd^{2+} display the conformations $S_4(2)$ or "$S_4(2)$" (9×), "$S_4(1)$" (1×), "$S_4(1)$"/"$D_{2d}(1)$" (2×), and C_1 (1×).[73] For 17 out of 20 complexes, the idealized symmetries are compatible with the symmetry predicted for either the global or the local minimum. The remaining three complexes are severely distorted and have low symmetries. The predicted global $D_{2d}(1)$ equilibrium conformation is found for one of the seven Fe^{2+} complexes in Table S.7, and the predicted global $S_4(2)$ conformation is found for 9 out of the 13 complexes with spherical metal ions. These data indicate that the relative stability of the two energy minima is occasionally altered by the crystalline environment. The external interactions responsible for these alterations include contributions such as Coulomb interactions with counterions, steric repulsions with cocrystallized molecules, Madelung energies, etc. In general, the crystalline environment does not only affect the relative energies of the conformations but also may distort the structure, leading to a distribution in the values for ω (cf., section 3.6.3) or to symmetry lowering. Complexes with large ligand residues are especially vulnerable in this respect.

The complex $[Cd(SC_6H_4\text{-}2\text{-}SiMe_3)_4]\cdot[NEt_4]_2$ presents an interesting case because it is the first example of a complex with a spherical metal ion that is locked in the $S_4(1)$ conformation.[74] The $Cd(SC)_4$ core of the complex (ω = 34.7°, see Table S.7) is nearly congruent with the $Fe(SC)_4$ core at the local $\omega \approx 35°$ minimum in Figure 4A and supports the notion that structurally competent S···S′ lone-pair interactions are a common feature of $[M(SR)_4]^{n-}$ complexes.

3.6.3. Relation between Bond Angle δ and Torsion Angle ω. The $\delta-\omega$ plot of the complexes listed in Table S.7 (Figure S.8) reveals that systems with $\omega < 80°$ (labeled (1)) have FeS_4 cores that are elongated along the S_4 axis ($\delta < 0°$) while those with $\omega > 80°$ (labeled (2)) have compressed cores ($\delta > 0°$).[75,76] The empirical correlation is in agreement with DFT (Figures 4C and S.5) and with the

(73) Symmetries of idealized structures of which the true symmetry is mostly C_1 have been listed in quotation marks. Multiple labels are assigned to complexes of which the idealized symmetry groups were ambiguous. $n\times$ means n occurrences.

(74) Block, E.; Gernon, M.; Kang, H.; Ofori-Okai, G.; Zubieta, J. *Inorg. Chem.* **1989**, *28*, 1263−1271.

(75) The complex $[Co(SC_6H_2\text{-}2, 4, 6\text{-}{}^iPr_3)_4]\cdot[NEt_4]$, which lies outside the plot boundaries, obeys the rule too.

(76) Fikar, R.; Koch, S. A.; Millar, M. *Inorg. Chem.* **1985**, *24*, 3311−3312.

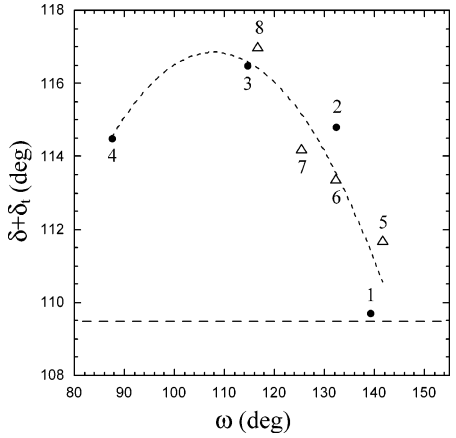

Figure 8. $\delta-\omega$ plot of the $[Fe(SR)_4]^{1-,2-}$ complexes in the Cambridge Crystallographic Database with (pseudo) S_4 symmetry. The dashed line indicates the tetrahedral angle, δ_t. The dotted curve is a parabola obtained by least-squares fitting of the data and is given by $\delta = 52.2 + 1.20\omega - 0.0056\omega^2$, with δ and ω in degrees (correlation coefficient is 0.91). Complexes: $[Fe^{III}(SEt)_4]^{1-}$ (1), $[Fe^{III}(SPh)_4]^{1-}$ (2), $[Fe^{III}(SMe)_4]^{1-}$ (3), $[Fe^{III}(SC_6HMe_4)_4]^{1-}$ (4), $[Fe^{II}(SEtOH)_4]^{2-}$ (5), $[Fe^{II}(Sbiph)_4]^{2-}$ (6), $[Fe^{II}(SC_6H_4NHCO^tBu)_4]^{2-}$ (7), and $[Fe^{II}(SC_6H_4Me)_4]^{2-}$ (8).

lone-pair repulsion model (Figure S.7B). As can be seen from Figures S.8 and S.9, the correlation is found in the crystallographic data for a wide range of metals, oxidation states, and residues, R. The universality corroborates the notion that the $\delta-\omega$ correlation originates from stereospecific S···S′ interactions, like those discussed in section 3.5. Despite the diversity of the complexes, the data points in Figure S.8 follow roughly the theoretical curve of Figure 4C. However, the dispersion in the data is large but improves significantly if one considers only complexes containing the same metal. This is shown for iron in Figure 8 where the data have been fitted with a parabolic curve, yielding the correlation coefficient $R = 0.91$. The right-most ferric complex, $[Fe(SEt)_4]\cdot[NPr_4]$,[16] has an almost tetrahedral FeS_4 core ($\delta \approx 0°$) because its torsion angle ($\omega \approx 139°$) is in the vicinity of a zero point in the $\delta_{min}(\omega)$ curve (see Figure 4C). As predicted by the theory, the experimental δ value increases for $\omega < 139°$, reaches a maximum at $\omega \approx 110°$ for $[Fe(SC_6H_4\text{-}4\text{-}Me)_4]\cdot 2[NEt_4]$,[77] and decreases again at $\omega = 87.5°$ for $[Fe(SC_6H\text{-}2,3,5,6\text{-}Me_4)_4]\cdot[NEt_4]$[78] (Figure 8). There are no complexes with torsion angles between 80° and 40°. Complexes with torsion angles in this region would be thermodynamically unstable because of the presence of a maximum in the lone-pair repulsion energy (see Figures 4A and S.7A).

Our explanation for the relationship between δ and ω differs from the one proposed by Coucouvanis et al. for the $\delta-\omega$ relation in the subset of $[Fe(SR)_4]^{n-}$ complexes, in which residue R is an aryl group.[15] These authors ascribed the δ distortions to steric repulsions between the sulfurs and the ortho hydrogens of the aryl residues. For example, repulsive forces between the ortho hydrogens of SPh(1) and SPh(2) and the sulfurs of SPh(3) and SPh(4) in the $D_{2d}(1)$ conformation tend to make the ∠S(1)FeS(2) angle smaller and lead to elongation, $\delta < 0°$. However, a quantitative assessment of the effect is lacking. The values of the shortest H···S distance in the complexes of Table S.7 are within 0.2 Å of the sum, 3.05 Å, of the van der Waals (VdW) radii for S and H.[79] One could speculate that the molecular geometries have relaxed to the point that any overlap between the VdW spheres of *o*-H and S is removed so that the VdW spheres, at most, only touch. Pursuing this line of argument, it is conceivable that steric interactions between the sulfurs and the hydrogens in R are the driving force behind the δ changes that lead to the $\delta-\omega$ correlation in Figure 8. However, there is a number of convincing arguments against this proposition: similar δ changes are found in geometry optimizations of complexes with both H-containing and H-free residues (Table 2), showing that the presence of hydrogens is a dispensable condition for having δ distortions; the alkyls (Me, Et, EtOH) lie approximately on the same curve as the aryl complexes in the $\delta-\omega$ plot of Figure 8, suggesting that the δ-distortion mechanism is independent of the structure of the ligand residues, R; given that the H···S distances in $[M(SR)_4]^{n-}$ complexes, R being an alkyl or aryl group, depend on a considerable number of structural variables, it seems unlikely that minimization of the steric repulsion energy of the H···S contacts would result in a unique correlation between δ and ω; and furthermore, the likelihood that such a relationship would resemble the $\delta-\omega$ plot obtained by the lone-pair repulsion model is even more remote.

Finally, we note that ω and δ are soft coordinates and are, therefore, both susceptible to distortions under the influence of the host in which the complex is placed.[80] However, since the molecular shape is primarily determined by ω and only to a lesser extent by δ, the crystallization (or incorporation) process utilizes, above all, the torsion angles for fitting the complexes into a periodic array (or protein). Once the value of ω is fixed by the crystalline (or protein) host, δ relaxes according to the intrinsic relationship, $\delta = \delta_{min}(\omega)$ (Figure 8).

4. Conclusion

The lone pairs of the thiolates in $[M(SR)_4]^{n-}$ play a pivotal role in the stereochemistry of these complexes due to their contributions to both the metal−ligand and ligand−ligand interactions. The interaction energy of the lone pairs with the $3d^6$ shell of high-spin Fe^{II} has a global, $D_{2d}(1)$ minimum with state $^5A_1(z^2)$ and a local, $S_4(2)$ minimum with state $^5B(x^2 - y^2, xy)$. The stereochemistry of complexes containing the spherical, high-spin, $3d^5$ ion Fe^{III} is determined by the electrostatic repulsions between the ligands. The lone-pair repulsions yield a global, $S_4(2)$ minimum and a local, $S_4(1)$ minimum, each with state ^6A. Since the local and global minima are close in energy, the Fe^{II}/Fe^{III} complexes can be locked into either of the equilibrium conformations under

(77) Kang, B.; Cai, J. *Jiegou Huaxue (J. Struct. Chem.)* **1985**, *4*, 119−122.
(78) Millar, M.; Lee, J. F.; O'Sullivan, T.; Koch, S. A.; Fikar, R. *Inorg. Chim. Acta* **1996**, *243*, 333−343.
(79) Hamilton, W. C.; Ibers, J. A. *Hydrogen Bonding in Solids*; Benjamin, Inc.: New York, 1968.
(80) DFT frequency calculations show that the force constants for ω and δ are small.

the influence of a crystalline host. The lone-pair repulsions distort the MS_4 core and give rise to a relationship between the ∠SFeS′ angles (δ) that are bisected by the S_4 axis and the torsion angle (ω): $\delta = \delta_{min}(\omega)$. The MS_4 unit is predicted to be elongated along the S_4 axis in the $D_{2d}(1)$ and $S_4(1)$ conformations and compressed in the $S_4(2)$ conformation. The theoretical relationship $\delta_{min}(\omega)$ is confirmed by crystallographic data.

Acknowledgment. This research was supported by National Science Foundation Grant MCD 9416224 (E.M.) and by National Institutes of Health Grant EB001475 (E.M.).

Supporting Information Available: Figures S.1−9, Tables S.1−7, and sections S.1−6. This material is available free of charge via the Internet at http://pubs.acs.org.

IC040049W